

# Performance enhancement of a PEM fuel cell through reactant gas channel and gas diffusion layer optimisation

S. O. Obayopo, T. Bello-Ochende and J. P. Meyer

*Department of Mechanical and Aeronautical Engineering, University of Pretoria,  
Pretoria 0002, South Africa*

Centre for Renewable and Sustainable Energy Studies

## Abstract

Proton exchange membrane fuel cells have many distinctive features that made it an attractive alternative clean energy source, including low start-up, high power density, high efficiency, portability and remote applications. Researches are on-going to improve its performance and reduce cost of this class of energy systems. In this work, a systematic procedure to optimize PEM fuel cell gas channels in the systems bipolar plates with the aim of globally optimizing the overall system net power performance at minimised pressure drop was carried out. In addition, the effect of various gas diffusion layer (GDL) properties on the fuel cell performance was examined. Simulations were done ranging from 0.6 to 1.6 mm for channel width, 0.5 to 3.0 mm for channel depth and 0.1 to 0.7 for the GDL porosity. The results indicate that effective design of reactant gas channel and GDL properties enhances the performance of the fuel cell system. The numerical results computed agree well with experimental data in the literature. Consequently, the results obtained provide useful information for improving the design of fuel cells.

Keywords: Proton exchange membrane; fuel cells; optimization; gas channel; performance

## 1. Introduction

Proton exchange membrane fuel cells (PEMFCs) using hydrogen are some of the emerging fuel cells with many advantages ranging from emission of water as waste, operation at low temperatures for quick start-up, and use of solid polymers as electrolytes, reducing both construction and safety complications (Du and Jana, 2007). This fuel cell type is seriously being considered as an alternative power source for stationary and mobile applications but there are several technical challenges which have to be overcome before it can be adopted for use in these devices.

One of the means of reducing the cost of PEMFCs is by improving their performance through system optimisation. This facilitates the understanding of how different parameters affect the performance of the fuel cell in real operating conditions and subsequently reduce the cost involved in prototype development. Much research has been carried out on PEMFCs ranging from one-dimensional models showing phenomena where mass transport limitations are taken into account and two or three-dimensional models encompassing thermal and water management. A vast number of previous works are CFD based (Yuan *et al.* 2010; Zhang and Jia, 2009; Obayopo *et al.* 2011). Available experimental work to date has been conducted mostly to validate highly sophisticated CFD simulations against the cell global polarisation curves (Cheddie and Munroe, 2007; Ferng *et al.*, 2008).

An issue of significant importance in PEM fuel cells is the pressure drop, especially at the cathode side of the cell. The product water generated at the cathode channel must be removed from the cell and this requires a high pressure drop. Also, too high pressure drops creates excessive parasitic power requirement for the pumping of air through the

cells. Hence, the effective design of the fuel channel is required to ensure a balance in pressure drop requirements at the fuel cell cathode section.

<b>Nomenclature</b>	
$a$	channel width (m)
$A_c$	cross-sectional area (m <sup>2</sup> )
$b$	channel depth (m)
$C$	constant
$D$	gas diffusivity (m <sup>2</sup> s <sup>-1</sup> )
$D_{eff}$	effective diffusivity (m <sup>2</sup> s <sup>-1</sup> )
$D_h$	hydraulic diameter (m)
$f$	friction factor
$I$	exchange current density (A m <sup>-2</sup> )
$L$	channel length (m)
$\dot{m}$	channel mass flow rate (kg/s)
$P$	pressure (Pa)
$P^*$	wetted perimeter
$Re$	Reynolds number
$T$	temperature (K)
$V$	cell potential (V)
<b>Greek</b>	
$\Delta$	difference operator
$\varepsilon$	porosity
$\mu$	fluid viscosity (kg m <sup>-1</sup> s <sup>-1</sup> )
$\rho$	density (kg m <sup>-3</sup> )
$\tau$	tortuosity
$\delta$	thickness (mm)
<b>Subscripts</b>	
avg	average
c	capillary
eff	effective
max	maximum
opt	optimum
GDL	gas diffusion layer
MEA	membrane electrode assembly
PEM	proton exchange membrane

Liu *et al.* (2007) studied two-phase flow and water flooding of reactants in the cathode flow channels of an operating transparent PEMFC experimentally. The effect of flow field type, cell temperature, cathode flow rate and operation time on water build-up and cell performance was studied. The results indicate the adverse effect of liquid water accumulation on mass transport and the subsequent reduction of the performance of the fuel cell.

Rodatz *et al.* (2004) conducted studies on the operational aspects of a PEMFC stack under practical conditions. Their study focused particularly on the pressure drop, two-phase flow and effect of bends. They observed a decrease in the pressure drops at a reduced stack current.

Maharudrayya *et al.* (2006) studied the pressure drop and flow distribution in multiple parallel channel configurations used in PEMFC stacks. Through their study, they

developed an algorithm to calculate the flow distribution and pressure drop in multiple U- and Z-type flow configurations of fuel cell.

Ahmed and Sung (2006) also performed a numerical model to investigate the performance of PEMFC at high operating current densities for various channel cross-sectional configurations while maintaining the same reactant flow rates and inlet boundary conditions. The results obtained reveals that rectangular channel cross-sections gave higher cell voltages, but the trapezoidal channel cross-section gave more uniform distributions at the membrane-cathode GDL interface. Their result further reveals the presence of an optimum channel-shoulder ratio for optimal fuel cell performance.

Most of the existing models in the literature address the effect of fuel channel geometric parameters on the performance of the PEM fuel cell without investigating the mutual interdependence of the GDL porous medium, reactant gas flow rate and gas channel geometry on the fuel cell system performance. Studies on PEM fuel cell performances, which incorporate the determination of optimal operating values for fuel cell design parameters taking into consideration the combined mutual effect of channel geometry, flow rate, and GDL characteristics, are still very limited in the literature. A good understanding of the interactive interdependence of these fuel cell parameters is therefore essential for optimum fuel cell design.

Therefore, the purpose of this study is to investigate the mutual effect of a range of operating conditions such as reactant flow rates, fuel channel geometry, and GDL parameters on the performance of a single PEM fuel cell and also to determine the optimal operating conditions for this class of fuel cell which has not been given much attention in the literature. The results are aimed at adding to the knowledge base needed to produce generic design information for fuel cell systems, which can be applied to better designs of fuel cell stacks.

## 2. MODEL DESCRIPTION

Figure 1 depicts the computational domain consisting of the anode flow channel, anode diffusion layer, MEA assembly, cathode diffusion layer, and cathode flow channel. In this model, the numerical domain is a full single-cell geometry domain. Pure hydrogen and air were used as reactant gases in the model. The inlet flow velocity was controlled by stoichiometry numbers of 1.2 at the anode and 2.0 at the cathode. The operating pressure was 101 kPa absolute at the exit of the cell. The details of the flow field and other physicochemical parameters used for the base case are summarised in Table 1 and Table 2. The detail governing equations that apply to the transport and gas mixtures in the fuel cell system for the model are presented in the author's previous work (Obayopo *et al.*, 2011). In the modelling of the fuel cell the following assumptions were made: the cell operates under steady-state conditions, isothermal boundary conditions were used for external walls, the flow in the cell is considered to be laminar, reactant and products are assumed to be ideal gas mixtures, and the electrode is assumed to be an isotropic and homogeneous porous medium.

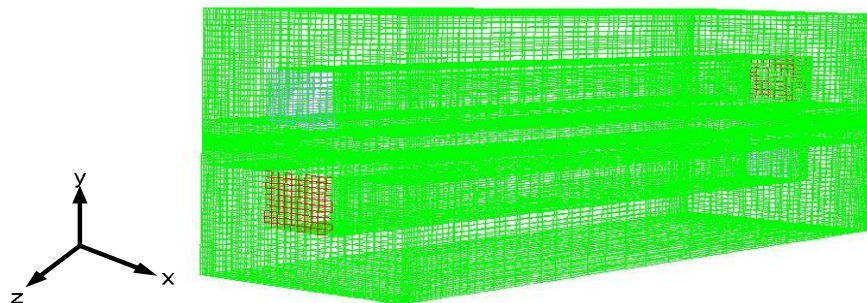


**Figure 1. The discretised three-dimensional computational domain of a single PEM fuel cell**

**Table 1. Base case geometric parameters of the modeled fuel cell**

Description	Value
Channel length (mm)	120
Channel width (mm)	1.0
Channel depth (mm)	1.2
Membrane thickness (mm)	0.036
Catalyst layer thickness (mm)	0.012
Electrode thickness (mm)	0.21

**Table 2. Physicochemical properties of the modeled fuel cell**

Description	Value
Cell operating temperature (°C)	70
Air-side/fuel-side inlet pressure (atm)	3/3
Open-circuit voltage (V)	0.95
Porosity of gas diffuser layer	0.4
Permeability of gas diffuser layer (m <sup>2</sup> )	1.76 x 10 <sup>-11</sup>
Tortuosity of gas diffuser layer	1.5
Porosity of catalyst layer	0.4
Permeability of catalyst layer (m <sup>2</sup> )	1.76 x 10 <sup>-11</sup>
Tortuosity of catalyst layer	1.5
Porosity of membrane	0.28
Permeability of membrane (m <sup>2</sup> )	1.8 x 10 <sup>-18</sup>
Reference diffusivity of H <sub>2</sub>	11 x 10 <sup>-5</sup> m <sup>2</sup> s <sup>-1</sup>
Reference diffusivity of O <sub>2</sub>	3.2 x 10 <sup>-5</sup> m <sup>2</sup> s <sup>-1</sup>
Electric conductivity of catalyst layer (Ω <sup>-1</sup> m <sup>-1</sup> )	190
Electric conductivity of GDL (Ω <sup>-1</sup> m <sup>-1</sup> )	300
Electric conductivity in carbon plate (Ω <sup>-1</sup> m <sup>-1</sup> )	4000
O <sub>2</sub> stoichiometry ratio	1.2
H <sub>2</sub> stoichiometry ratio	2.0
Oxygen mole fraction	0.406
Relative humidity of inlet fuel/air	100%
Reference current density of anode (A/m <sup>2</sup> )	7 500
Reference current density of cathode (A/m <sup>2</sup> )	20
Anode transfer coefficient	2.0
Cathode transfer coefficient	2.0

## 2.1 Channel cross-section

Flow channels in fuel cells are typically rectangular in cross-section, though other configurations such as triangular, trapezoidal, and semi-circular have been explored for fuel cell designs (Hontanon *et al.*, 2000). The manufacturing processes of the flow channels in fuel cell are quite time-consuming and expensive since graphite, which is hard

and brittle, is typically used as the material of choice. Hence the making of the flow channel is a major cost in the development of a complete PEM fuel cell. In the design of small fuel cells, where the pressure drop is of the order of 0.5-1 bar, serpentine or interdigitated channels could be applicable but in larger fuel cells, this is not possible as the pressure drop would be in the order of a few bars (Maharudrayya *et al.*, 2004). From cost considerations, manufacturing and performance requirements, the geometrical shape of the channel cross-section has traditionally been either rectangular or square. The rectangular cross-section was used in the design of the PEM fuel cell in this study and is schematically shown in Figure 2. For internal flows such as the ones in fuel cell channels, the Reynolds number is conventionally defined as (White, 1986):

$$Re_{D_h} = \frac{\rho V_{avg} D_h}{\mu} \quad (1)$$

$$V_{avg} = \frac{\dot{m}}{\rho A_c} \quad (2)$$

For a rectangular channel in this study,  $D_h$  is defined as (White, 1986):

$$D_h = \frac{4A_c}{P^*} \quad (3)$$

For the channel under consideration in Figure 2, the cross-sectional area is equal to the product of the channel width and the channel depth.

$$A_c = ab \quad (4)$$

and the wetted perimeter is

$$P^* = 2(a + b) \quad (5)$$

The pressure drop for a flow in a channel of length  $L$  is usually expressed using the following relation (White, 1986):

$$\Delta p = f \frac{L}{D_h} \frac{\rho V_{avg}^2}{2} \quad (6)$$

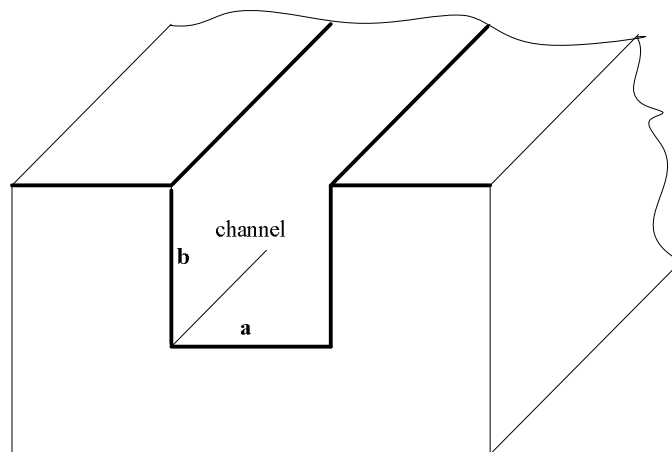


**Figure 2. Channel cross-sectional view.**

where the friction factor  $f$  for steady fully developed laminar flows in a channel with square cross-section is given as

$$f = \frac{56.91}{Re_{D_h}} \quad (7)$$

Substituting the above relation Eq. (7) into Eq. (6), and taking into consideration Eqs. (1) to (5), the pressure drop can be obtained for flow channels with square cross-section ( $a = b$ ), as

$$\Delta P = 28.455 \left( \frac{\mu \dot{m}}{\rho} \right) \left( \frac{L}{a^3} \right) \quad (8)$$

Thus the flow channel length for flow channels with a square cross-section can be determined as

$$L = \frac{\Delta p \rho a^3}{28.455 \mu \dot{m}} \quad (9)$$

Similarly, we can obtain the flow channel length for a rectangular cross-section as

$$L = \frac{8 \Delta p \rho (ab)^2}{C \mu \dot{m} (a+b)^2} \quad (10)$$

where  $C = f Re_{D_h}$  is a function of the  $b/a$  for rectangular flow channels (White, 1986).

The pressure drop in the channel can be obtained using the flow rate ( $q$ ) – pressure drop  $\Delta P$  relationship for a rectangular cross-section relation (White, 1991):

$$q = \frac{4ba^3}{3\mu} \times \frac{-\Delta P}{\Delta L} \left[ 1 - \frac{192}{\pi^5 b} \sum_{i=1,3,5..}^{\infty} \frac{\tanh(i\pi b/2a)}{i^5} \right] \quad (11)$$

## 2.2 Fluid flow through GDL

In fuel cells, the fluid flow diffuses through the GDL for the reaction to take place on the MEA. The effective diffusivity for gas-phase flow in porous media can be written as:

$$D_{eff} = \frac{D}{\tau} \quad (12)$$

The tortuosity ( $\tau$ ) is a difficult parameter to estimate except through experiment. Hence it is usually correlated in fuel cell studies using a Bruggeman correlation. This correlation assumes  $\tau$  is proportional to  $\varepsilon^{-0.5}$  resulting in the simpler expression (Mench, 2008):

$$D_{eff} = D \varepsilon^{1.5} \quad (13)$$

The porosity correlation is used to adjust for the longer effective path length through the porous media.

## 2.3 Boundary conditions

Pressure boundary conditions were specified at the outlets since the reactant gas flow is usually separate and at different pressures. The inlets were all assigned as mass flow inlets. The gas diffusion layer and the catalyst layer were surrounded by sealed plates at the inlet and outlet planes, so the boundary conditions at the inlet and outlet planes take the no-slip condition for the velocity and non-permeable condition for the species mass fraction. The membrane-electrode interface was defined as a wall, primarily to inhibit

species and electron crossover through the membrane. This also prevents pressure problems at the interface. In the areas at which the gas diffusion electrodes were in contact with the bipolar plates, a constant reference voltage equal to zero was assigned as a boundary condition both at the anode and at the cathode. The electron flux was set to zero at all other walls. The anode was grounded ( $V = 0$ ) and the cathode terminal was set at a fixed potential (0.75 V) less than the open-circuit potential (0.95 V). Both anode and cathode terminals were assigned wall boundaries.

## 2.4 Solution technique

The model equations were solved using the CFD software ANSYS Fluent® 12.0 with Gambit® (2.4.6) as a pre-processor. The CFD code has an add-on package for fuel cells, which has the requirements of the source terms for species transport equations, heat sources and liquid water formations (Ansys, 2009). Control volume technique was used for solving the problem. The meshes were more refined at the membrane-catalyst assembly regions. The conservation of mass, momentum and energy equations in the three-dimensions were solved, in turn, until the iterative process met the convergence criteria. In this study, the definition of convergence criteria indicates that the largest relative error between two consecutive iterative residuals within the overall computational domains is less than  $10^{-6}$ .

The domain was divided into hexahedral volume elements. A computational mesh of about 257 346 volume elements was obtained with the grid. The grid independence was verified at the preliminary test runs. Four structured grid configurations were evaluated for the PEMFC. The number of elements in the  $x$ -,  $y$ -, and  $z$ - directions was: (a)  $70 \times 70 \times 25$ , (b)  $87 \times 87 \times 34$ , (c)  $104 \times 87 \times 34$  and (d)  $104 \times 104 \times 43$ . The influence of the number of elements on the local current density at an operating voltage of 0.4 V was investigated. The local current density for grid (a) differs from that of (b-d) with deviation of about 4.2%. However, the local current density distributions for grids (b), (c) and (d) do not show any significant differences. The difference between the local current densities for (b) and (c) is about 0.36% and the difference between (c) and (d) is 0.48%. Grid (c) was chosen for the simulations as a trade-off between accuracy and cost of time. The solution strategy was based on the SIMPLE algorithm (Pantakar, 1980).

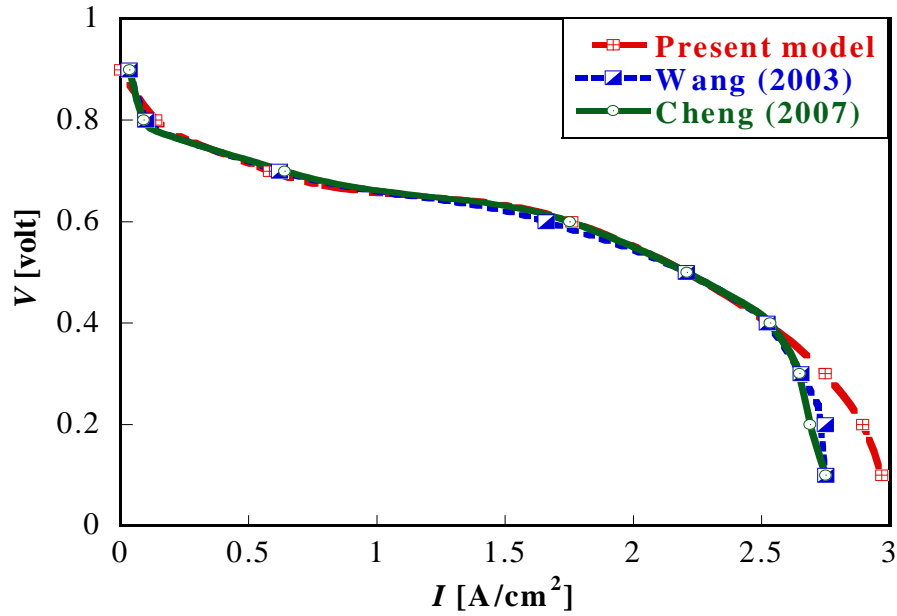
## 2.5 Model validation

The validation of physical and numerical models is very important; hence comparison with some experimental data is highly desirable. The simulation results for the base case operating conditions were verified against experimental measurements of Wang *et al.* (2003) and Cheng *et al.* (2007). The computed polarisation curve shown in Figure 3 is in good agreement with the experimental curves in the low load region. However, the model current density in the high mass transport limited region ( $> 2.75 \text{ A/cm}^2$ ) is higher than the experimental values. This observation is common in models where the effect of reduced oxygen transport due to water flooding at the cathode at higher current density cannot be properly accounted for (Berning and Djilali, 2003). Nonetheless, the prediction from the model could still successfully be used for better understanding of the complicated processes in fuel cell systems.

## 3. Results and Discussions

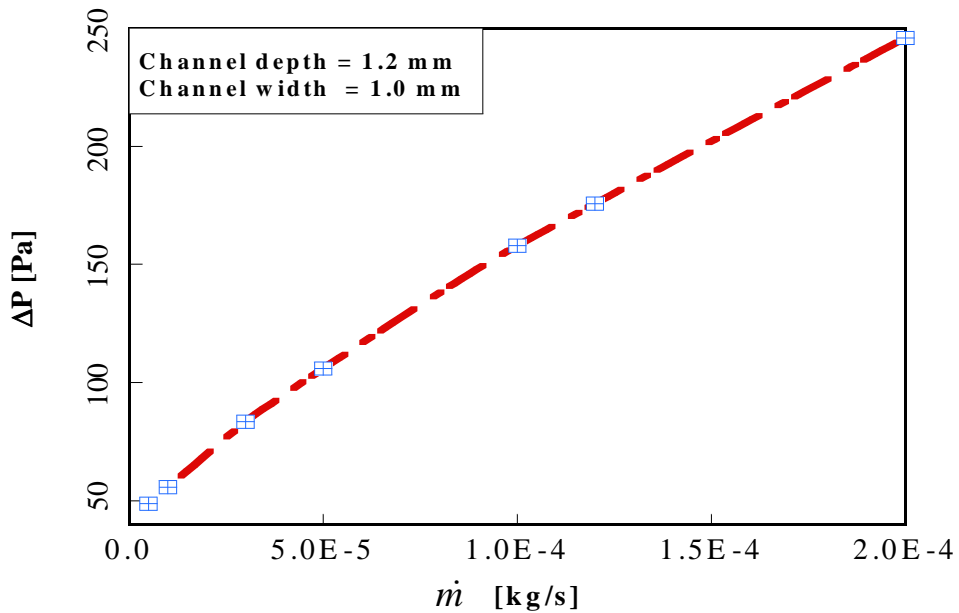
### 3.1 Pressure drop in flow channel

Figure 4 shows the calculated pressure drops for the rectangular flow channel over a range of air mass flow rates at a channel depth and width of 1.2 mm and 1.0 mm, respectively. The results indicate that the pressure drop increases as the mass flow rate at the cathode is increased. This is expected since an increase in the mass flow rate increases the reaction of the reactant species and also reduces the resident water in the cathode channel of the fuel cell. Generally, fuel cells with high pressure drops in the flow



**Figure 3. Comparison of numerical model prediction and experimental polarisation curves at base condition.**

field exhibit a more even distribution of the reactant species flow than those with low pressure drops in their flow fields. These even distributions do greatly enhance the fuel cell performance (Labaek *et al.* 2010).



**Figure 4 Pressure drop along the model flow channel at base operating conditions for a channel depth of 2.0 mm and width of 1.2 mm.**

### 3.2 Effect of physical parameters on PEM fuel cell performance

Figure 5 shows the effect of changing the oxygen mass flow rate from 5.0E-06 to 1.6E-04 kg/s on the fuel cell performance. When the cathode gas mass flow rate is increased, the fuel cell performance is enhanced especially at lower operating fuel cell voltages.

The reason is the increase in oxygen gas through the gas diffusion layer to the reaction sites, which increases the rate of reaction. At low operating voltages, more liquid water is produced due to stronger electrochemical reaction rates, which is expected to reduce fuel cell performance. However, the high oxygen mass flow rates in the porous layer generate high shear forces, which aid the transport of liquid water downstream at the flow channel along the flow direction. The effect is minimal at high operating voltages as observed on the curves primarily due to low membrane humidification. Wang and Liu (2004) obtained similar results in their experimental work on PEM fuel cell performance. This is because low amount of water presence occurs at these voltage levels due to slow reaction rates coupled with an increase in the oxygen gas supply resulting in reduced cell performance.

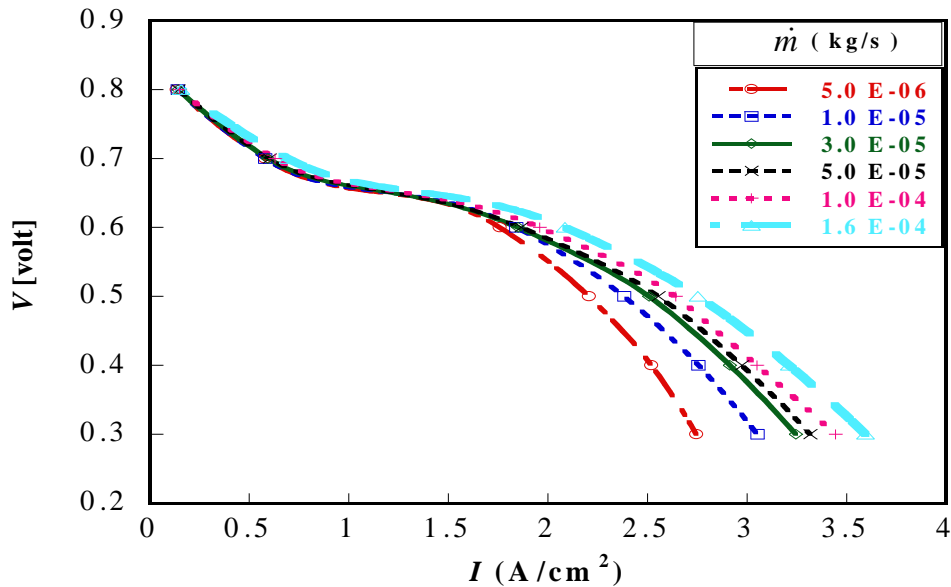


**Figure 5. Effect of cathode gas flow rate on cell performance at base conditions.**

The effect of the gas diffusion layer porosity on the performance of the PEM fuel cell is shown in Figure 6. The results show the fact that the effect of gas diffusion layer porosity on fuel cell performance is significant when the gas diffusion layer is in the low value region (0.1 to 0.4). Increasing the diffusion layer porosity size has an increasingly weaker effect on the performance. The gas diffusion layer porosity beyond 0.6 does not have a significant effect on the fuel cell polarisation curve. This observation is in agreement with optimisation work of Lin *et al.* (2006). They reported an optimum GDL porosity of 0.5913 for PEM fuel cell modeled in their study. Therefore, maintaining porosity levels between 0.4 and 0.6 will be a reasonable value for the fuel cell if durability issues in the fuel cell structure are to be taken into consideration.

The effect of the gas diffusion layer thickness is shown in Figure 7. A thin layer of the gas diffusion layer improves the gas diffusion into the reaction sites and also facilitates water removal thereby improving the fuel cell performance. Figure 7 shows a decreasing fuel cell performance for an increasing GDL thickness. Increasing the GDL thickness hampers the gas distribution onto the membrane sites thereby hindering effective reaction in the fuel cell system.

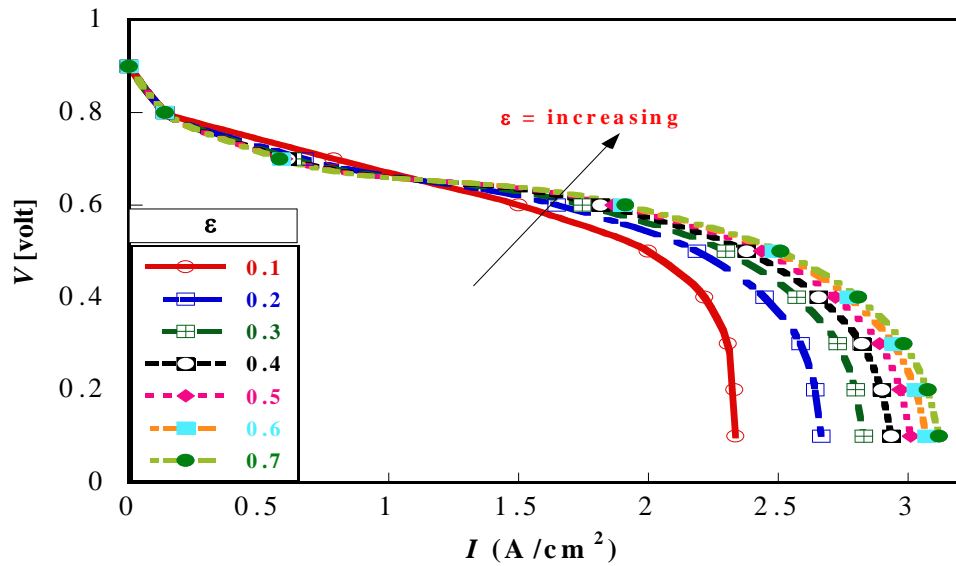


**Figure 6. Effect of gas diffusion layer porosity on cell performance at base conditions.**

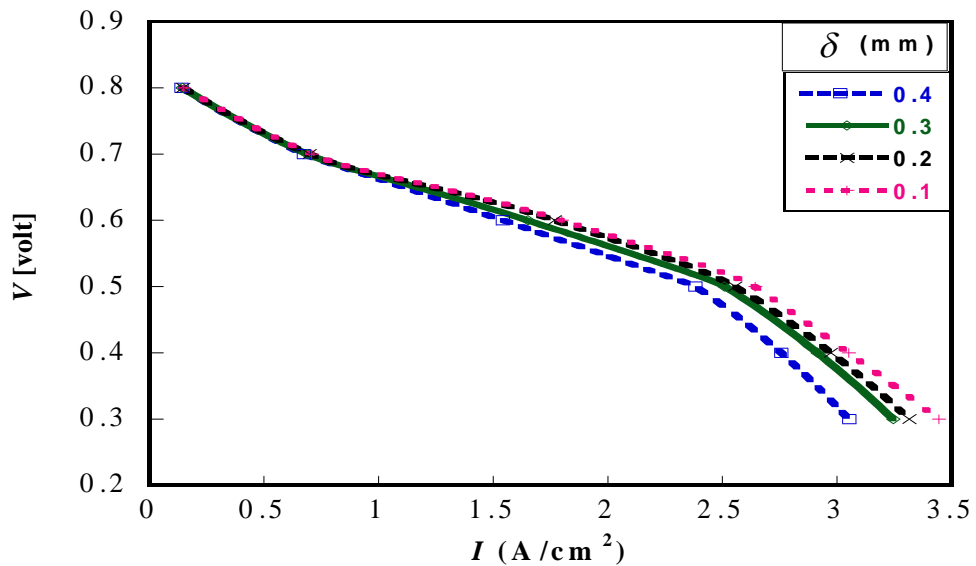


**Figure 7. Effect of gas diffusion layer thickness at the base case conditions for a porosity of 0.3 and a mass flow rate of 5E-06 kg/s.**

### 3.3 Effect of design parameters on PEM fuel cell performance

Simulations were performed for different sets of channel dimensions. Two different parameters which are channel width and channel depth were chosen for the study. Figure 8 illustrates the effect of channel depth on the fuel cell performance at a constant channel length. The optimal current density for the fuel cell was obtained at a channel depth of 2.0 mm (current density: 2.62 A/cm<sup>2</sup>). A further increase in depth showed a decline in fuel cell performance.

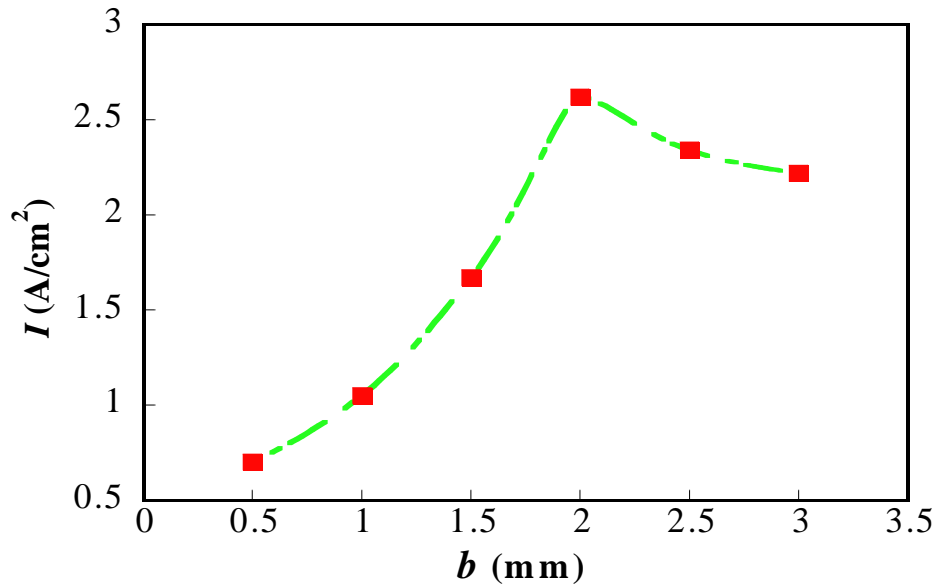


**Figure 8.** The cell current density at different channel depths at a cell potential of 0.3V and a mass flow rate of 5E-06 kg/s.

Figure 9 shows the fuel cell performance for the six cases of channel widths considered. Performance increased gradually from case 1 (0.6 mm – current density: 1.30 A/cm<sup>2</sup>) until an optimum was obtained at case 4 (1.2 mm – current density: 2.45 A/cm<sup>2</sup>). Increasing the channel width beyond 1.2 mm showed a reduction in fuel cell performance. These results were consistent with those observed by other researchers. Watkins *et al.* (1991) studied optimal dimension for cathode-side channels. They claimed that the most preferred ranges are 1.02 - 2.04 mm for channel depths and 1.14 - 1.4 mm for channel widths. Figures 9 and 10 suggest the existence of an optimal channel depth and width for the PEM fuel cell that will offer best system performance.

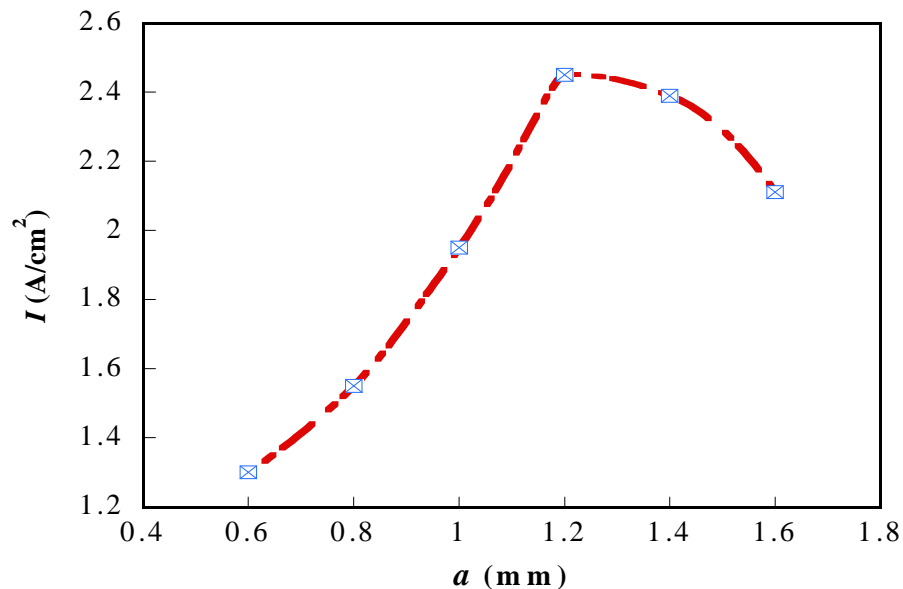


**Figure 9.** The cell current density at different channel widths at a porosity of 0.3 and a mass flow rate of 5E-06 kg/s.

### 3.4 Optimal channel geometry

The results in section 3.3 (Figures 8 and 9) depicts the existence of an optimal channel depth and width for a PEM fuel cell system. The search for an optimal channel depth and

width was carried out for the PEM fuel channel at varying GDL porosities. The first run of the simulation was carried out by fixing the cathode gas flow rate at  $5\text{E-}06$  kg/s, width of channel at 1.2 mm, cell operating voltage at 0.3 V and gas diffusion layer porosity at 0.2. The channel depth was then varied between 0.5 and 3.0 mm. An optimal channel depth,  $b_{opt}$ , was found for this configuration. The procedure was repeated for other values of gas diffusion layer porosities in the range of  $0.2 \leq \epsilon \leq 0.6$  as shown in Figure 10, until an optimal channel depth, which corresponds with the maximum current density, was obtained at each value of the gas diffusion layer porosity.

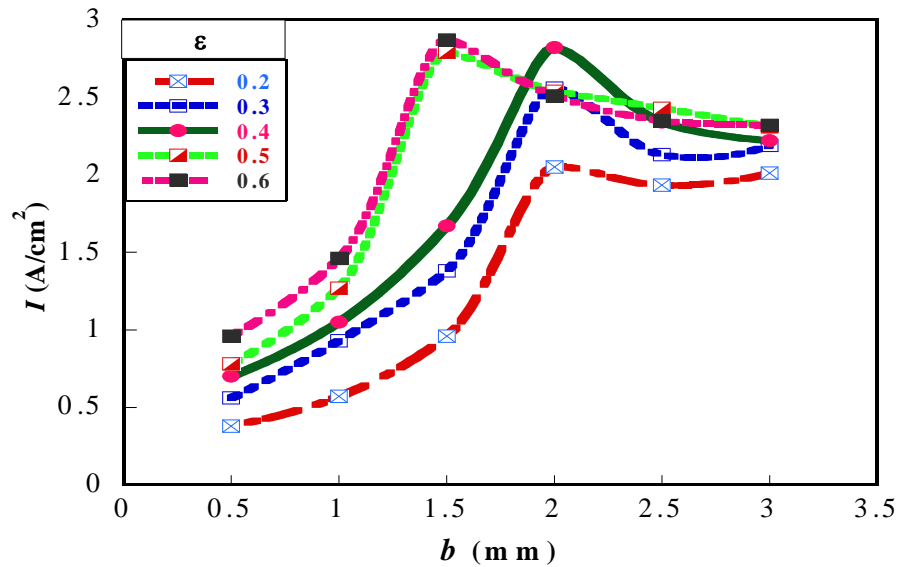


**Figure 10. Effect of porosity and channel depth on the cell current density for a mass flow rate of  $5\text{E-}06$  and a width of 1.2 mm.**

Figure 11 gives the optimum channel depth,  $b_{opt}$ , for different cathode gas mass flow rates for different gas diffusion layer porosities. The optimal channel depth decreases as the mass flow rate increases.

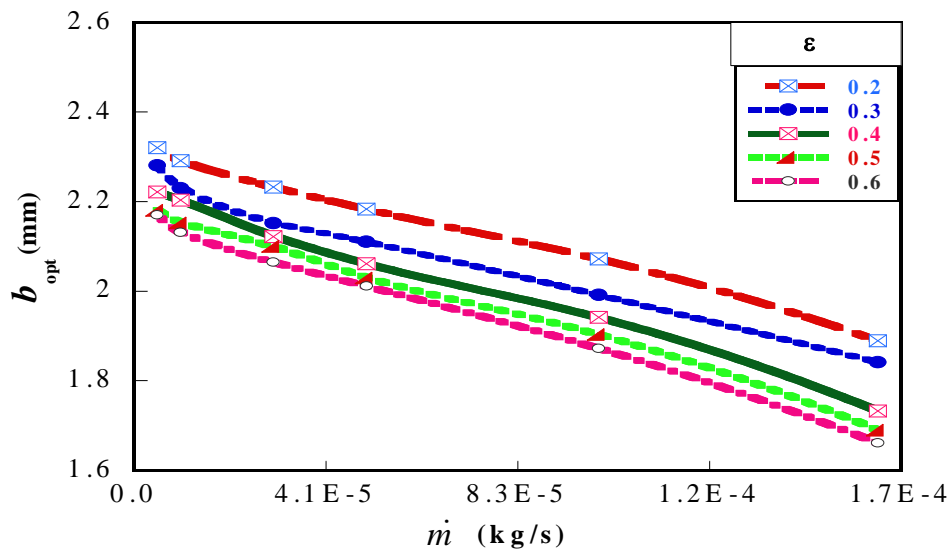


**Figure 11. Optimum depths as a function of flow rate and gas diffusion layer porosity.**

Figure 12 shows the behaviour of the maximum current density,  $I_{max}$ , with varying cathode gas mass flow rates. Each point of the figure depicts the result of a full

optimisation with respect to channel depth. The graph shows that maximised current density increases as the mass flow rate of the reactant gas increases. In each case, there is an optimal channel depth that maximises the current density of the fuel cell.

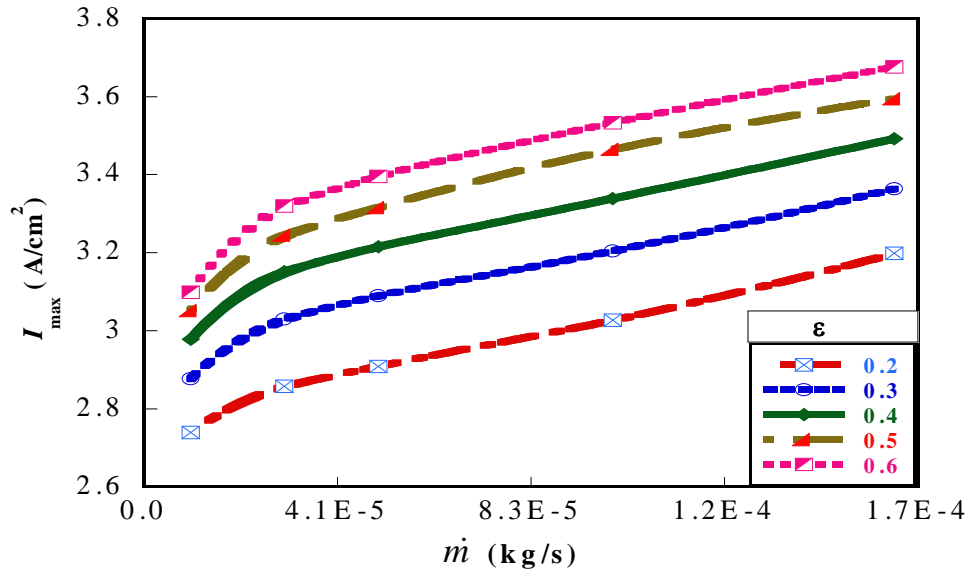


**Figure 12. Effect of flow rate and gas diffusion layer porosity on the cell current density.**

Similarly, the search for optimal channel widths,  $a_{opt}$ , corresponding to the maximum current density,  $I_{max}$ , was carried out as conducted for the channel depths. Figure 13 shows the current density value as a function of the channel widths for different values of gas diffusion layer porosities. The cathode gas mass flow rate and channel depth were initially fixed at  $5e-06$  kg/s and 2.0 mm, respectively.

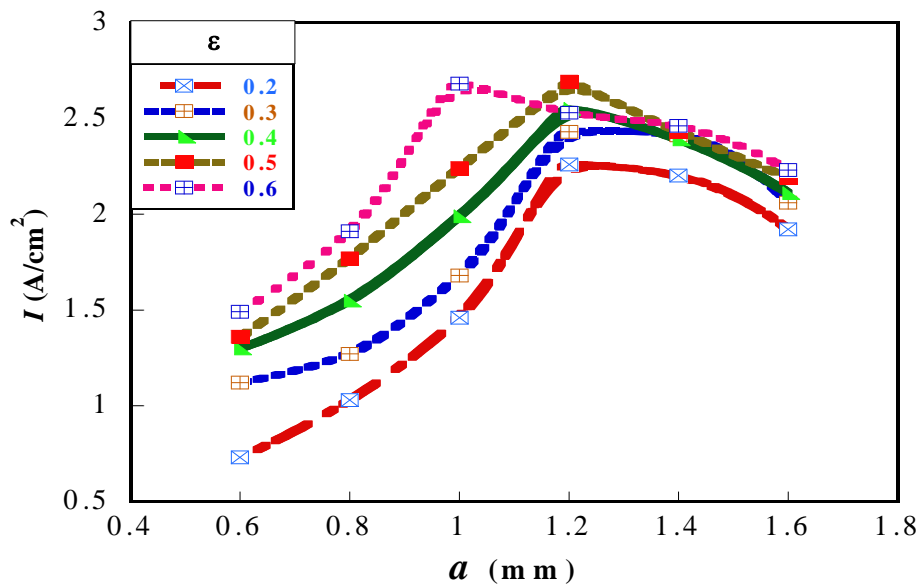


**Figure 13. Effect of porosity and channel width ( $b = 2.0$  mm) on the cell current density for mass flow rate of  $5E-06$  kg/s.**

Figure 14 depicts the optimal value of the channel width as a function of the cathode gas mass flow rate for each of the values of gas diffusion layer porosities ( $0.2 \leq \epsilon \leq 0.6$ ). The optimal channel widths,  $a_{opt}$ , from the figure decreases as the mass flow rate increases. The results obtained from Figures 11 and 14 both suggest that optimal channel depth and width decrease at increasing cathode gas mass flow rates. In designing PEM fuel cells it

can be concluded that matching the fuel cell operating conditions and the gas fuel channel configuration is very important for optimum operation issues.

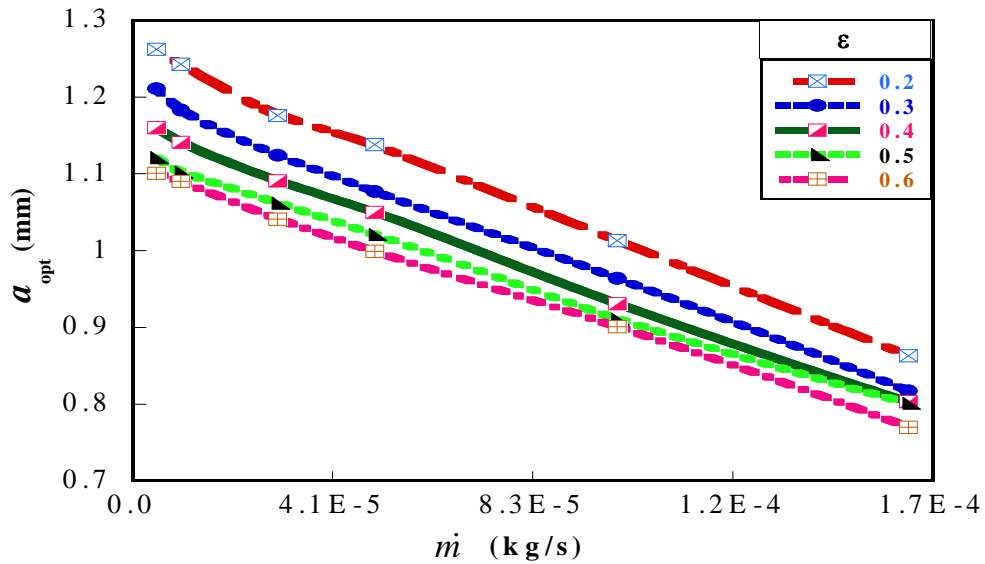


**Figure 14. Optimum widths as a function of flow rate and gas diffusion layer porosity.**

#### 4. Conclusions and recommendations

In this paper, a steady-state three-dimensional computational model was established to study the performance of a single channel proton exchange membrane fuel cell under varying operating conditions. The model prediction was validated by comparison with experimental data and was in good agreement. The results show that gas diffusion layer porosity, thickness and cathode gas mass flow rate affect the performance of the fuel cell. The porosity effects on fuel cell performance are more significant at porosity level of 0.1 to 0.4 than at porosity levels of 0.5 to 0.7. Increase in the GDL thickness also reduces gas reactant diffusion and subsequently reduce fuel cell performance. This study establishes the need to match the PEM fuel cell parameters such as porosity, species reactant mass flow rates and fuel gas channels geometry in the system design for maximum power output.

#### References

Ahmed, D.H., & Sung, H.J. 2006. Effects of channel geometrical configuration and shoulder width on PEMFC performance at high current density. *J. Power Sources* 162: 327-339.

Ansys Fluent® 12.0. 2009. Users Guide Documentation, Ansys Inc., Southpointe, SAS.

Berning, T., & Djilali, N. 2003. *J. Electrochem Soc.* 150(12): A1598-A1607.

Cheddie, D.F., & Munroe, N.D.H. 2007. A two-phase model of an intermediate temperature PEM fuel cell. *Int. J. Hydrogen Energy* 32: 832-841.

Cheng, C.H., Lin, H.H., & Lai, G. 2007. Design for geometric parameters of PEM fuel cell by integrating computational fluid dynamics code with optimisation method. *J. Power Sources* 165: 803-813.

Du, L., & Jana, S.C. 2007. Highly conductive/graphite composites for bipolar plates in proton exchange membrane fuel cells. *J. Power Sources* 172: 734-741.

- Ferng, Y.M., Su, A., & Lu, S.M. 2008. Experiment and simulation investigations for effects of flow channel patterns on the PEMFC performance. *International Journal of Energy Research* 32: 12-23.
- Hontanon, E., Escudero, M.J., Bautista, C., Garcia-Ybarra, P.L., & Daza, L. 2000. Optimization of flow-field in polymer electrolyte membrane fuel cells using computational fluid dynamics techniques. *J. Power Sources* 86: 363-68.
- Labaek, J., Bang, M., & Kaer, S.K. 2010. Flow and pressure distribution in fuel cell manifolds. *ASME J. Fuel Cell Sci. Technology* 7/061001-1.
- Lin, H.H., Cheng, C.H., Soong, C.Y., Chen, F., & Yan, W.M. 2006. Optimisation of key parameters in the proton exchange membrane fuel cell. *J. Power Sources* 162: 246-254.
- Liu, X., Guo, H., & Ma, C. 2007. Water flooding and pressure drop characteristics in flow channels of proton exchange membrane fuel cells. *Electrochim. Acta* 52: 3607-3614.
- Maharudrayya, S., Jayanti, S., & Deshpande, A.P. 2004 Pressure losses in laminar flow through serpentine channels in fuel cell stacks. *J. Power Sources* 138: 1-13.
- Maharudrayya, S., Jayanti, S., & Deshpande, A.P. 2006. Pressure drop and flow distribution in multiple parallel-channel configurations used in proton-exchange membrane fuel cell stacks. *J. Power Sources* 157: 358-367.
- Mench, M.M. 2008. *Fuel Cell Engines*. New Jersey: John Wiley & Sons
- Obayopo, S.O., Bello-Ochende, T., & Meyer J.P. 2011. Three-dimensional optimisation of a fuel gas channel of a PEM fuel cell for maximum current density. *International Journal of Energy Research* DOI:10.1002/er.1935.
- Pantakar, S.V. 1980. *Numerical Heat Transfer and Fluid Flow*. New York: Hemisphere.
- Rodatz, P., Buechi, F., Onder, C., & Guzzella, L. 2004. Operational aspects of a large PEFC stack under practical conditions. *J. Power Sources* 128: 208-217.
- Wang, L., Husar, A., Zhou, T., & Liu, H. 2003. A parametric study of PEM fuel cell performances. *Int. J. Hydrogen Energy* 28: 1263-1272.
- Wang, L., & Liu, H. 2004. Performance studies of PEM fuel cells with interdigitated flow fields. *J. Power Sources* 134:185-196.
- Watkins, D.S., Dircks, K.W., & Epp, D.G. 1991. Novel fuel cell fluid flow fieldplate. *US Patent* 4988583.
- White, F.M. 1986. *Fluid Mechanics*. New York: McGraw Hill
- White, F.M. 1991. *Viscous Fluid Flow*. New York: McGraw Hill.
- Yuan, W., Tang, Y., Pan, M., Li, Z., & Tang, B. 2010. Model prediction of effects of operating parameters on proton exchange membrane fuel cell performance. *Renewable Energy* 35: 656-666.
- Zhang, Z., & Jia, L. 2009. Parametric study of the porous cathode in the PEM fuel cell. *International Journal of Energy Research* 33: 52-61.